SCIENTIFIC REPORTS
nature research

OPEN

Efficient Sn Recovery from SnO_2 by Alkane ($C_xH_{y=2x+2}$, $0 \leq x \leq 4$) Reduction

Hyesung An[1,2], Mi Yoo[1,2], Hyunwoo Ha[1,2], Hyuk Choi[1], Eunji Kang[1] & Hyun You Kim[1*]

We study the mechanism of alkane reduction of SnO_2 for efficient low-temperature recovery of Sn from SnO_2. Based on thermodynamic simulation results, we comparatively analyze the reduction behavior and the efficiency of SnO_2 reduction by H_2 and alkanes ($C_xH_{y=2x+2}$, $0 \leq x \leq 4$). We found that alkanes ($n{\cdot}C_xH_y$) with the higher *nx* generally complete the reduction of SnO_2 (T_{100}) at the lower temperature. Moreover, the T_{100} of the SnO_2 reduction by alkanes ($n{\cdot}C_xH_y$) was decreased from the T_{100} of pure hydrogen with the same amount of hydrogen atoms ($n{\cdot}H_y$). We found that the concentration of a gas phase product mixture, the amount of the produced solid carbon, and the T_{100} complementary vary as a function of the *nx* and *ny*, the total amount of carbon and hydrogen atoms in the reducing gas phase molecules. Our results demonstrate a viability of the low temperature reduction method of SnO_2 by alkanes for efficient recovery of Sn from SnO_2, which can be applied for Sn recovery from Sn containing industrial wastes or Sn ores with economic value added that is held by the co-produced H_2.

Recovering (extracting) valuable metallic elements from industrial wastes is technically important for the efficient recycle of earth unabundant resources. However, the current dry-smelting, hydro-smelting, or combined smelting-electrolytic refining technologies, which are commonly applied for extraction of high purity metals from ores or used oxidized scraps, are not environmentally friendly[1–9]. Because the high quality minable ores deplete first, designing environmentally friendly techniques are necessary to set up ecofriendly recovery processes of used metals.

Although Sn (Tin) is relatively earth unabundant among the industrially demanded metals, Sn and Sn oxides play a key role in several electronic devices and products such as sensor[10,11], Pb-free solder[12,13], or transparent electrode[14–16]. Despite of the high LME (London Metal Exchange) market price ($16,450.00/metric ton as of October 4, 2019) of Sn[17], which is more than 3 and 1.5 times expansive than Cu and Ni, respectively, 70% of the annually consumed Sn is not appropriately recycled[18]. Recovery of Sn from used SnO_2 or oxidized metal scrap proceeds in a similar process with the ore smelting in the presence of a proper and strong reducer, usually cokes. However, a poor solid-solid contact between SnO_x and cokes and a high operation temperature lowers the overall efficiency[19].

In our previous report[20,21], we have designed a methane reduction (MR) method, an ecofriendly and simple versatile process of Sn recovery from SnO_x containing industrial wastes, which also can be potentially applied for Sn ore smelting. A direct facile contact between gas phase methane and SnO_x improves the efficiency of the reaction. Moreover, multiple reductants provided by methane (hydrogen and carbon) sequentially reduce SnO_x, producing H_2O, H_2, CO, or CO_2 depending on the reduction conditions[21]. The geometry of a SnO_2 bound methane inhibits the initial participation of the carbon of methane to the reduction process[21]. Rather, the released hydrogen atoms from methane attribute to the initial reduction power of methane[21]. The extended release of two kinds of reducing agents from methane assures the versatility of the MR of SnO_x and the increased economic efficiency[21]. Another interesting finding was that the H_2/CO ratio in the produced gas varies as a function of the CH_4/SnO_2 ratio. We found that the H_2/CO ratio increases if the MR of SnO_x proceeds under oxygen depleted conditions because the late released more oxophilic carbon takes up oxygen atoms from SnO_x and gas phase H_2O[21].

Unique chemistry between Sn and CH_4 has reported in a recent study by the Metiu and McFarland groups[22]. They found that molten Sn and other transition metals can directly dissociate CH_4 into solid C and H_2 and suggested that such direct H_2 production from CH_4 without CO_2 formation as an advanced H_2 production method

[1]Department of Materials Science and Engineering, Chungnam National University, 99 Daehak-ro, Yuseong-gu, Daejeon, 34134, Republic of Korea. [2]These authors contributed equally: Hyesung An, Mi Yoo and Hyunwoo Ha. *email: kimhy@cnu.ac.kr

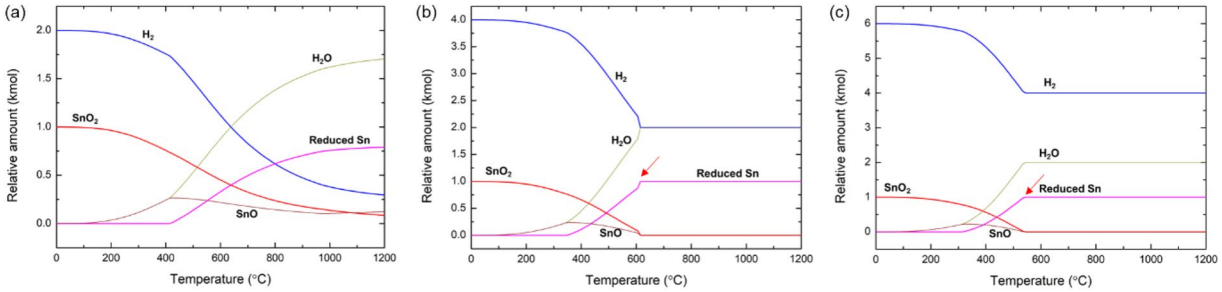

Figure 1. Theoretical prediction of the H_2 reduction of SnO_2. (**a**–**c**) Equilibrium concentration of the mixture of one mole of SnO_2 and n·CH_4 ($n = 2$, 4, or 6) as a function of temperature. (**a**) $H_2/SnO_2 = 2$, (**b**) $H_2/SnO_2 = 4$, and (c) $H_2/SnO_2 = 6$. The red arrows in (**b**) nd (**c**) indicated the T_{100}.

Amount of supplied H_2, n, (kmol)	2	4	6	8	9	10
T_{100} (°C)	n/a[a]	615	545	494	484	464

Table 1. T_{100} of n·H_2 reduction of SnO_2 as a function of the amount of supplied H_2, n. [a]Reduction was not completed up to 1200 °C.

from hydrocarbons[22]. Based on our previous findings on the CH_4 reduction of SnO_2[21], we have reached to a hypothesis that use of alkanes with more carbon and hydrogen contents per mole ($C_xH_{y=2x+2}$, $0 \le x \le 4$) would accelerate the SnO_2 reduction and also lower the reaction temperature. Moreover, if molten Sn, which is produced upon SnO_2 reduction by alkanes, assists dissociation of alkanes into carbon and hydrogen, the SnO_2 reduction would occur under the stronger reduction atmosphere so that the overall SnO_2 reduction will be greatly accelerated.

In this letter, we use a combined study of thermodynamic simulations and density functional theory (DFT) calculations to study the effect of the C/H_2 ratio in the reducing gas on the efficiency of the reduction of SnO_2. To provide a fundamental insight into the mechanism of SnO_2 reduction by alkanes with the higher carbon and hydrogen contents per mole and further clarify the reduction potential of the applied alkanes, we introduce commercially available alkanes ($C_xH_{y=2x+2}$, $0 \le x \le 4$) as a reducing agent for SnO_2 reduction. The efficiency of the alkane reduction of SnO_2 is evaluated by the reduction complete temperature, T_{100}, and compared with the T_{100} of mole-balanced pure hydrogen. We find that the T_{100} is an inverse exponential function of the amount of supplied reducing agent (H_2 or alkane) and that the addition of carbon as a form of alkane significantly lowers the T_{100} from that of the H_2 reduction of SnO_2. Our findings predict that the operation temperature of the alkane reduction of SnO_2 can be adjusted by controlling the composition and the x/y ratio of the reducing gas, suggesting an easy and industrially highly accessible recycling process of SnO_x containing industrial wastes.

Results and Discussion

H_2 reduction of SnO_2. Figure 1 shows the equilibrium concentrations of the mixture of SnO_2 and n·H_2 ($n = 2$, 4, or 6) at between 0 to 1200 °C. Obviously, H_2 reduces SnO_2 into Sn through a two-step process. In all cases, SnO_2 was first transferred to SnO. SnO was formed at below the melting temperature of Sn (231.9 °C) and further transferred to metallic Sn upon temperature increase. Under the stoichiometric condition ($H_2/SnO_2 = 2$, 2 moles of H_2 is required to reduce a mole of SnO_2 to Sn and $2H_2O$), the reduction does not complete even at 1200 °C and SnO survives. The T_{100}, at which SnO_2 and SnO were completely reduced to Sn, was significantly decreased upon increase of the amount of supplied H_2 up to 4 or 6 moles ($H_2/SnO_2 = 4$ or 6, respectively, Table 1). Because consistent two moles of H_2 were used for SnO_2 reduction to Sn, irrespective to the initial H_2/SnO_2 ratio, the decrease of the T_{100} is presumably due to the increased chemical potential of gas phase H_2 upon increase in the H_2/SnO_2 ratio.

Alkane reduction of SnO_2: methane and ethane. Figure 2 shows the equilibrium concentrations of the mixture of SnO_2 and n·CH_4 (Fig. 2a,b) or n·C_2H_6 (Fig. 2c,d) ($n = 2$ or 4) at between 0 to 1200 °C. Like the cases of the H_2 reduction of SnO_2, the T_{100} is equal to the point at which the SnO and SnO_2 are completely depleted. Because a mole of CH_4 supplies total five units of reducing agents (one C and four H), a mole of SnO_2 can be easily reduced to metallic Sn. The increase of H_2, C, and H_2O above 200 °C shows that CH_4 was decomposed into C and H_2 and the released H_2 from CH_4 initially reduces SnO_2. The delayed increase of CO_2 compared to the increase of C confirms that the reduction by C occurs at the higher temperature than the reduction by H_2. In both cases ($CH_4/SnO_2 = 2$ or 4) the decrease of H_2O, C, and CO_2 is coupled with the increase of CO and H_2, meaning that C takes up oxygen from SnO_2 under C and H_2 rich conditions. Despite the active role of hydrogen in the early stage of the reduction, carbon completes the reduction and hydrogen of CH_4 was released as gas phase H_2. The T_{100} of CH_4 reduction of SnO_2 also decreases response to the increase of the CH_4/SnO_2 ratio (Table 2).

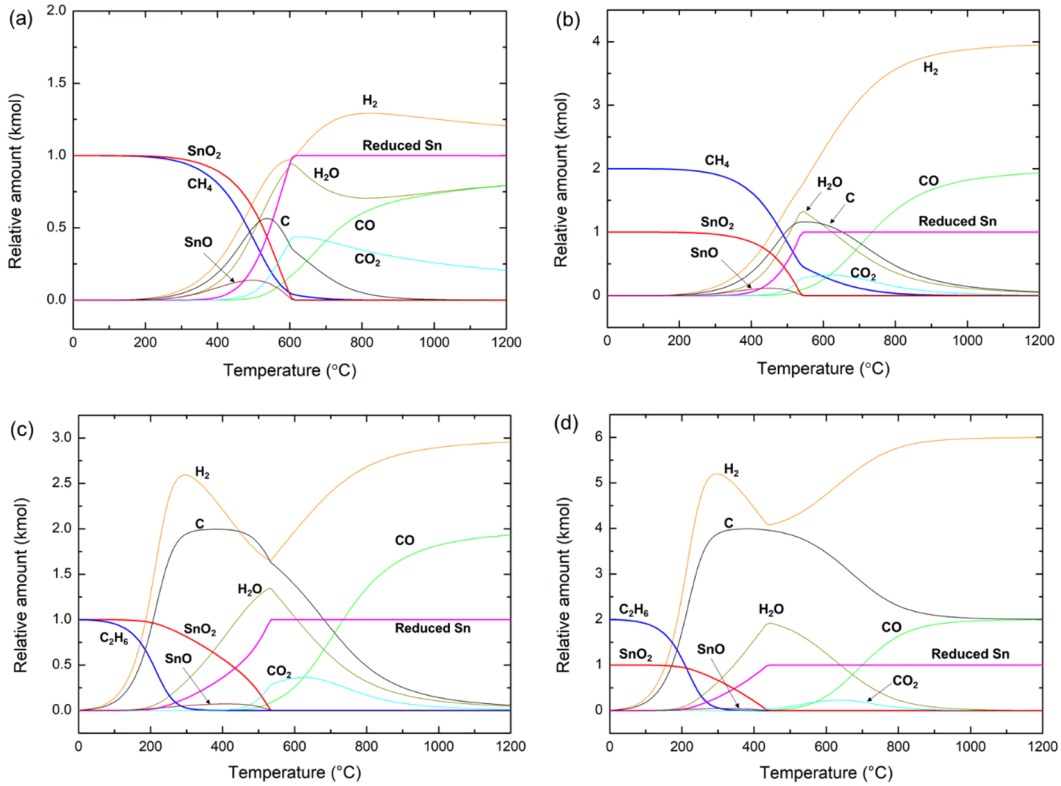

Figure 2. Temperature dependent evolution of equilibrium concentration of reactants and products during (**a**,**b**) CH_4 or (**c**,**d**) C_2H_6 reduction of SnO_2. (**a**) $CH_4 + SnO_2$, (**b**) $2CH_4 + SnO_2$, (**c**) $C_2H_6 + SnO_2$, and (**d**) $2C_2H_6 + SnO_2$.

n·$C_xH_{y=2x+2}$ ($x = 1$ or 2), (nx, ny) (kmol)	1·CH_4 (1, 4)	2·CH_4 (2, 8)	1·C_2H_6 (2, 6)	2·C_2H_6 (4, 12)
T_{100} (°C)	615	545	534	444

Table 2. T_{100} of n·$C_xH_{y=2x+2}$ ($x = 1$ or 2) reduction of SnO_2 as a function of the amount of supplied alkanes, n.

The overall reduction process, initial active reduction of SnO_2 by H_2 and complete reduction by C, was consistently appeared in the C_2H_6 reduction of SnO_2. C_2H_6 decomposes rapidly into C and H_2 and the overall reduction occurs under highly reducible conditions. However, although the reduction occurs under C and H_2 rich conditions, SnO was also appeared as an intermediate, showing that the reduction of SnO_2 occurs through a two-step process. The rapidly increased H_2 upon C_2H_6 decomposition gradually decreased as H_2 was transformed to H_2O. Like the case of CH_4 reduction of SnO_2, C takes up oxygen, being transformed to CO_2 and eventually, to CO. Most of the H_2 transformed to H_2O was released upon CO formation. When the C_2H_6/SnO_2 increases to 4, the excess C was remained as solid state carbon even after complete reduction of SnO_2. The T_{100} values of C_2H_6 reduction of SnO_2 were generally lower than the values of CH_4 reduction of SnO_2 (Table 2). The effect of the amount of C and H_2 in reducing alkanes on the T_{100} will be discussed below.

Alkane reduction of SnO_2: propane and butane. C_3H_8, propane, and C_4H_{10}, butane, are commercially widely available alkanes and a component of liquid petroleum gas. No meaningful changes in the reduction behavior was observed in the C_3H_8 and C_4H_{10} reduction of SnO_2 (Fig. 3). Decomposition of C_3H_8 and C_4H_{10} caused a rapid increase of H_2 and C in the initial state of the reduction. Gradual increase of H_2O coupled with the increase of reduced Sn and SnO represents the initial reduction of SnO_2 by H_2 released from alkanes. Because the excess amount of H_2 was supplied, even in the presence of solid state carbon, H_2 takes up oxygen from SnO_2. Subsequent reactions between H_2O and solid state carbon produce CO_2, CO, and H_2. Eventually, all of the oxygen from SnO_2 was converted to CO at high temperatures and the excess C and all of H_2 from alkanes were released as is. Upon increase of the supplied C_3H_8 and C_4H_{10}, the T_{100} was also significantly reduced (Table 3). Interestingly, the formation of SnO was suppressed at $C_3H_8/SnO_2 = 2$ and $C_4H_{10}/SnO_2 = 2$. Direct reduction of SnO_2 could become available under H_2 rich conditions.

Modelling the reduction trend in alkanes (n·$C_xH_{y=2x+2}$, $0 \leq x \leq 4$). The equilibrium concentration diagrams presented in Figs 1 and 2 show that the overall reduction process of SnO_2 by H_2 and alkanes (n·$C_xH_{y=2x+2}$, $0 \leq x \leq 4$) does not differ a lot. Vigorous release of H_2 at low temperatures from alkanes generates the similar reducing atmosphere with the reduction by pure H_2. Addition of the released C from alkanes induces the

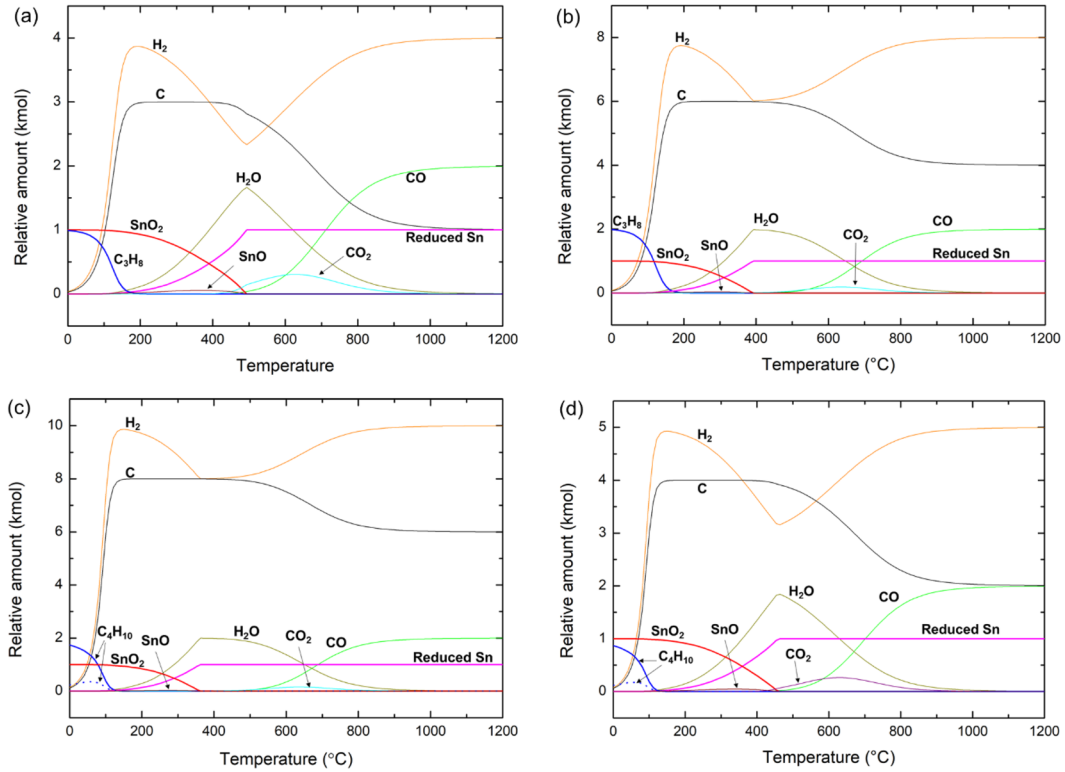

Figure 3. Temperature dependent evolution of equilibrium concentration of reactants and products during (**a**,**b**) C_3H_8 or (**c**,**d**) C_4H_{10} reduction of SnO_2. (**a**) $C_3H_8 + SnO_2$, (**b**) $2C_3H_8 + SnO_2$, (**c**) $C_4H_{10} + SnO_2$, and (**d**) $2C_4H_{10} + SnO_2$.

n·$C_xH_{y=2x+2}$ ($x = 3$ or 4), (nx, ny) (kmol)	1·C_3H_8 (3, 8)	2·C_3H_8 (6, 16)	1·C_4H_{10} (4, 10)	2·C_4H_{10} (8, 20)
T_{100} (°C)	494	393	464	363

Table 3. T_{100} of n·$C_xH_{y=2x+2}$ ($x = 3$ or 4) reduction of SnO_2 as a function of the amount of supplied alkanes, n.

gas phase conversion of H_2O into H_2. Moreover, as the alkane/SnO_2 ratio increases from 1 to 2, the T_{100} decreases. The response of the T_{100} as a function of the total amount of supplied C, nx, and H, ny, is presented in Tables 2, 3 and Fig. 4a.

Considering that the T_{100} values are exponentially decreasing upon increase of nx and ny and that the addition of C affects to the T_{100}, we presented the T_{100} values as a function of nx (Fig. 4b) or ny (Fig. 4c). Figure 4b shows that once the amount of C, nx, is given, the T_{100} just slightly varies upon change in ny, presenting the quite prominent and dominant effect of C on the T_{100} of SnO_2 reduction by alkanes, as predicted by thermochemical data: the standard formation enthalpy of CO_2, $\Delta H_f^0(CO_2, 298.15\ K) = -393.474$ kJ/mol, is greater than that of water, $\Delta H_f^0(H_2O, 298.15\ K) = -285.830$ kJ/mol[23]. Because single C atom can take over two O atoms from SnO_2, whereas two H atoms are required to remove one O atom from SnO_2, C of alkanes will naturally more aggressively reduce SnO_2.

In Fig. 4c, to more intensively compare the effect of C on the T_{100} of SnO_2, we presented a pair of dataset, the T_{100} values of H_2 or alkane reduction of SnO_2 as a function of ny. The control group data, the T_{100} values acquired from H_2 reduction of SnO_2, gradually decrease as a function of ny: 615 °C at $H_2/SnO_2 = 8$ and 464 °C at $H_2/SnO_2 = 20$. The filled square data points in Fig. 4c represent the T_{100} of SnO_2 reduction by n·CH_4, n·C_2H_6, n·C_3H_8, and n·C_4H_{10}. For the cases where two or more combinations of alkanes are available to match the total amount of supplied hydrogen, ny, we took the case with the higher nx. For example, we took the T_{100} from $2C_2H_6$ ($nx = 4$) rather than that from $3CH_4$ ($nx = 3$), to compare with the T_{100} from $6H_2$ ($ny = 12$). The T_{100} values of alkane reduction of SnO_2, fitted to an exponential function, show a significantly decrease in T_{100} (Fig. 4c). Replacing a reducing agent from 4 moles of H_2 ($ny = 8$) to a mole of C_3H_8 ($nx = 3$, $ny = 8$) decreased the T_{100} of a mole of SnO_2 from 615 °C to 494 °C (Fig. 4c). The fitted exponential curves of T_{100} as a function of nx or ny (solid lines in Fig. 4b,c) show that the T_{100} of the alkane or H_2 reduction can be fit to simple exponential functions (refer to Tables 4 and 5 for fitting constants and R^2-values).

Interestingly, we found that the ΔT_{100} (T_{100}-alkane – T_{100}-hydrogen), an indicator of the effect of carbons from alkanes on the reduction of SnO_2 was −121 °C at $ny = 3$ and rapidly saturated to −101 °C at $ny = 4$ and beyond (Fig. 4c). The ΔT_{100} calculated from the two fitted exponential curves predicts the slightly fluctuating ΔT_{100}

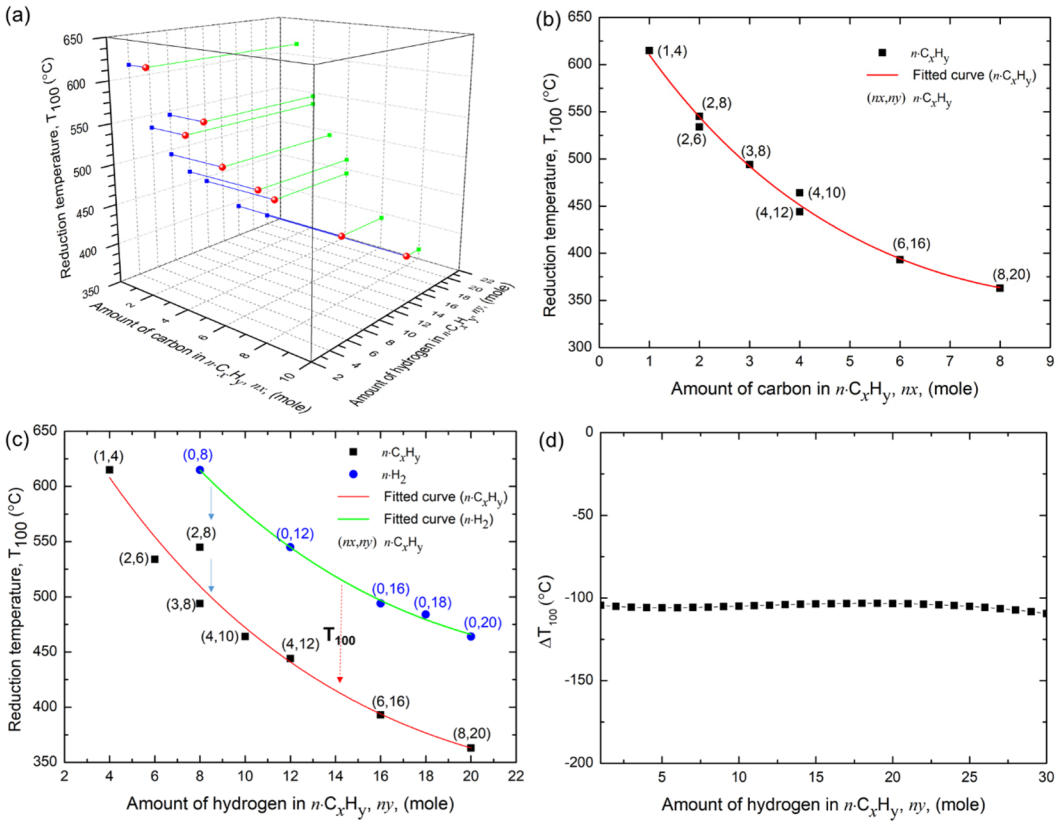

Figure 4. Effect of C on the T_{100} of H_2 or alkane reduction of SnO_2. (**a**) A 3-dimensional diagram of T_{100} of alkane reduction of SnO_2 presented as a function of *nx* and *ny*. (**b**) T_{100} values of alkane reduction of SnO_2 plotted as a function of *nx*. The pairs of numbers in the parentheses present the total units of C, *nx*, and H, *ny*, in alkanes. (**c**) T_{100} values of H_2 or alkane reduction of SnO_2 plotted as a function of *ny*. The pairs of numbers in the parentheses present the total units of C, *nx*, and H, *ny*, in reductants. Red and green lines present the fitted exponential functions of T_{100} as a function of *ny*. (**d**) ΔT_{100} values estimated from the two fitted exponential curves of T_{100}.

Reference function	$T_{100} = exp[a + b\,(nx) + c(nx)^2]$, $(1 \leq nx \leq 10)$			
Fitting parameters	**a**	**b**	**c**	**Adjusted R^2**
$\underline{n}$·C_xH_y reduction of SnO_2	6.5413	−0.1340	0.0067	0.9898

Table 4. T_{100} of alkane reduction of SnO_2 fitted to an exponential function of *nx*.

Reference function	$T_{100} = exp[a + b\,(ny) + c(ny)^2]$, $(0 \leq ny \leq 20)$			
Fitting parameters	a	b	c	Adjusted R^2
H_2 reduction of SnO_2	6.7477	−0.0479	8.8363×10^{-4}	0.9956
$\underline{n}$·C_xH_y reduction of SnO_2	6.6350	−0.0629	0.0013	0.9834

Table 5. The T_{100} of H_2 or alkane reduction of SnO_2 fitted to an exponential function of *ny*.

centered at −105 °C (Fig. 4d). Because the ΔT_{100} was estimated comparing the (0, *ny*) and (*nx*, *ny*) data points with the maximum *nx* value, it naturally represents the maximum effect of C addition to the T_{100} of SnO_2 reduction. The overall increase of *nx* and *ny* is beneficial for SnO_2 reduction because the lower T_{100} assures the higher economic efficiency. However, the effect of additional C to the T_{100} is limited to $\Delta T_{100} \approx -105$ °C. The vertically separated three data points in Fig. 4c, (0, 8), (2, 8), and (3, 8), show that the effect of C on the T_{100} increase as a function of C addition. Because C released from alkanes aggressively attack H_2O and liberate hydrogens of H_2O, the presence of excess C may increase the chemical potential and the reducing potential of gas phase H_2[21].

Reaction mechanism of alkane reduction of SnO_2. As a prototypical example of alkane reduction of SnO_2, DFT-calculated reaction mechanism of CH_4 reduction of SnO_2 is presented in Fig. 5a. The original DFT-calculated reaction energy values were adopted from our previous publication (Under Creative Commons

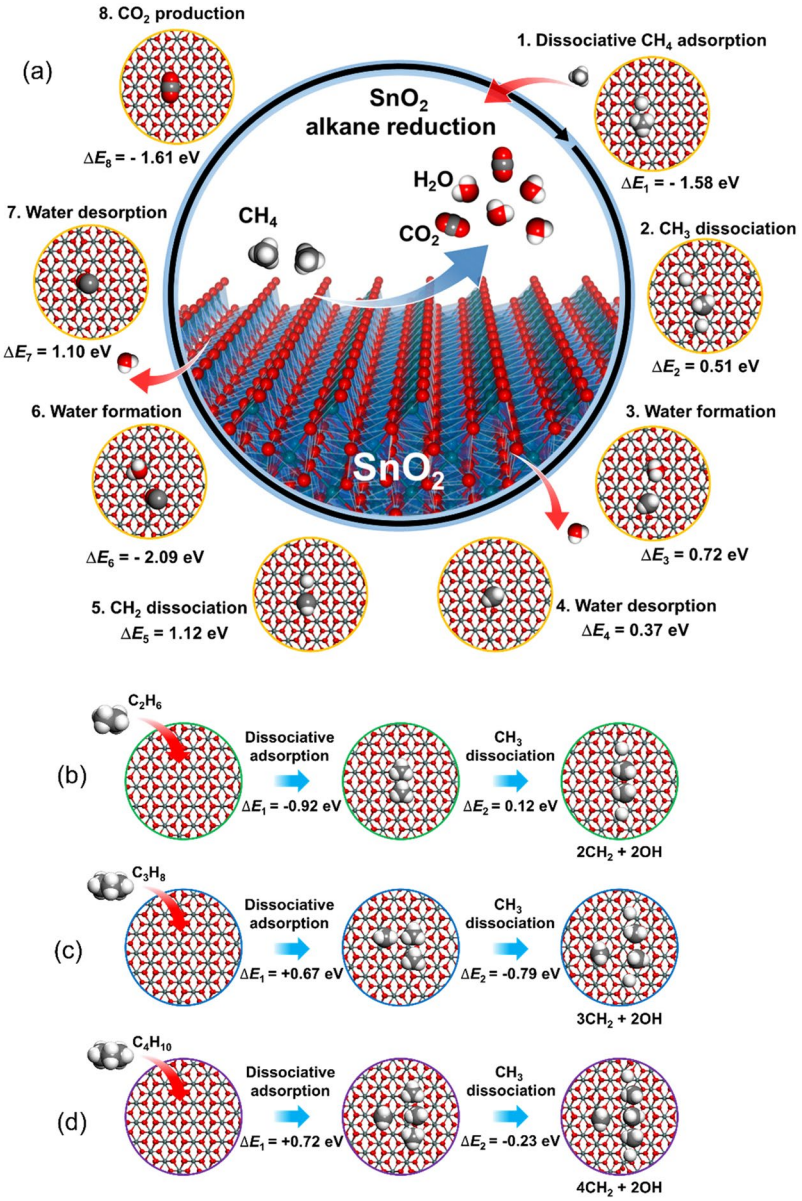

Figure 5. DFT-estimated mechanism of alkane reduction of SnO_2. (**a**) CH_4 was introduced as a prototypical alkane molecule to explore the atomistic mechanism of alkane reduction of SnO_2. The reduction reaction proceeds clockwise following the numerical order. ΔE_n presents the energetics of the n^{th} process. White and grey spheres denote hydrogen and carbon atoms, respectively. Sn and oxygen atoms are colored in deep green and red, respectively. Because of the protruded hydrogen atoms of a methyl group, $-CH_3$, formed upon dissociative adsorption of CH_4, initially participate in the reduction process, H_2O is the initial product. The original data for the reaction pathway and the morphology of each reaction stage are adopted from our previous report (ref.[21]). Dissociative adsorption of (**b**) C_2H_6, (**c**) C_3H_8, and (**d**) C_4H_{10} on $SnO_2(100)$. Dissociative adsorption of alkanes of $2 \leq x \leq 4$ produces multiple –OH and $-CH_3$ groups. Because each $-CH_3$ group was eventually dissociated into $-CH_2$ and –OH, the mechanism and the energetic of the subsequent reactions follow the case presented in panel (a).

Attribution 4.0 International License)[21]. The initial CH_4 dissociative adsorption (Process #1, Fig. 5a) initiates the CH_4 reduction of SnO_2. Because a CH_4 molecule was dissociated into a $-CH_3$ methyl group and a hydrogen atom, which are independently bound to surface lattice oxygen atoms of SnO_2, the SnO_2 surface will be strongly hydrogenated upon exposure to CH_4. The sequential combined processes of dehydrogenation of $-CH_3$ to –CH (Processes #2 to #5) and water formation (process #3 and #4) are energetically uphill. This is because two hydrogen atoms produced upon dehydrogenation of single CH_4 molecule were used for water formation. As we discussed above, under the CH_4 rich reduction conditions, the surface oxygen ions of SnO_2 will be eventually hydrogenated and thus the endothermic dehydrogenation of $-CH_3$ and water formation will not hinder the overall reduction of SnO_2. The second water formation (Process #6 and #7) and CO_2 production (Process #8) are

strongly thermodynamically preferred. The overall reduction of SnO_2 by CH_4 shows that the hydrogen atoms of CH_4 participate in the reduction process first and the residual carbon atom finally reduces SnO_2. This finding is consistent with the equilibrium concentration diagrams (Figs 2 and 3) showing that H_2O always forms first to CO and CO_2.

Interestingly, upon initial adsorption of C_2H_4, C_3H_8, and C_4H_{10}, multiple –OH and $–CH_3$ groups were formed as a result of dissociative adsorption of alkanes (Fig. 5b–d). Later, each $–CH_3$ group was eventually dissociated into $–CH_2$ and –OH, therefore the subsequent $–CH_2$ dissociation, water formation, and CO_2 formation processes would saturate into the same processes presented in Fig. 5a. The overall reaction mechanism of SnO_2 reduction by alkanes ($C_xH_{y=2x+2}$, $0 \le x \le 4$), therefore, is identical to each other except for the detailed energetics of the initial dissociative binding step. Interestingly, the initial dissociative adsorption of C_3H_8 and C_4H_{10} are energetically endothermic (Fig. 5c,d). However, considering that the alkane reduction would occur under the high alkane partial pressure conditions[20,21], the highly negative entropic contribution to the Gibbs free energy of binding, $-T\Delta S$, will definitely compensate the positive ΔE of dissociative adsorption (ΔE_1 in Fig. 5c,d)[24,25], making the ΔG of dissociative C_3H_8 and C_4H_{10} binding negative (exothermic). The roughly calculated highly negative $-T\Delta S^0$ at standard state[26] of propane (−0.83 eV) and butane (−0.95 eV) confirm that the ΔG values of dissociative alkane bindings ($\Delta G = \Delta E - T\Delta S$) are negative. The DFT-calculated mechanism of alkane ($C_xH_{y=2x+2}$, $0 \le x \le 4$) reduction of SnO_2 shows that the overall reaction mechanism is consistent within the alkanes that we applied ($C_xH_{y=2x+2}$, $0 \le x \le 4$) for SnO_2 reduction, irrespective to x and y. This result confirms that the significantly accelerated reduction potential of alkanes upon increase in nx is due to the quantitatively excessive supply of reducing agents by alkanes with the higher nx. As we have noticed in the introducing part, the presence of the already reduced liquid Sn metal may assist the direct reduction of alkanes. If this process occurs, the overall reaction will proceed under the higher H_2 partial pressure conditions (under the total pressure greater than 1 atm) with excessive solid state carbon supply. Results on the mechanism of SnO_2 reduction by alkanes under the various conditions (partial pressure and carbon content) will be reported in due course.

Conclusions

We study the mechanism of alkane reduction of SnO_2 for efficient low-temperature recovery of Sn from SnO_2 using combined study of thermodynamic simulations and DFT calculations. Through a comparative analysis of the reducing power of H_2 and commercially available alkanes ($C_xH_{y=2x+2}$, $0 \le x \le 4$) toward SnO_2 reduction, we scaled the reducing potential of studied reductants with T_{100}, the temperature at which SnO_2 is completely converted to metallic Sn. The alkanes with the higher nx and ny quickly complete the reduction at low T_{100}. Moreover, the positive effect of nx on the T_{100} was quite prominent in all studied cases of alkane reduction of SnO_2. The T_{100} of the SnO_2 reduction by alkanes ($n{\cdot}C_xH_y$) was significantly decreased from the T_{100} of pure hydrogen with the same amount of hydrogen atoms ($n{\cdot}H_y$). The fitted exponential curves of T_{100} plotted as a function of ny, presents that the effect of C on the T_{100} being saturated to $\Delta T_{100} \approx -105$ °C.

The C and H atoms released from alkanes sequentially reduce SnO_2 to Sn and eventually to metallic Sn. The initial stage of SnO_2 reduction by alkane is identical to the H_2 reduction of SnO_2; H_2 takes up oxygen from SnO_2. However, in the presence of the released C from alkanes, H_2 of H_2O is released as a gas phase molecule as C takes up oxygen from H_2O. Because the gas phase redistribution between H_2O, H_2, CO, and CO_2, caused by solid C occurs at above the T_{100}, the role of the solid C released from alkanes is likely to adjust the chemical potential of hydrogen of H_2O and H_2, accelerating the reduction of SnO_2 by H_2. The DFT-calculated atomic scale mechanism of alkane reduction of SnO_2 confirmed that the overall reaction mechanism is consistent within applied alkanes ($C_xH_{y=2x+2}$, $0 \le x \le 4$).

Our results show that the alkane reduction of SnO_2 is an effective recovery method of metallic Sn from SnO_2 or SnO containing industrial wastes or from Sn ores. The low T_{100} values of alkane reduction and the maximum ΔT_{100} of −105 °C suggest that the alkane reduction of SnO_2 assures high economically efficiency with economic value added that is held by the co-produced H_2 and carbons.

Methods

Thermodynamic simulation. Thermodynamic simulations were performed with the HSC 6.0 code (Outotec Research, www.hsc-chemistry.com). The relative thermodynamic stability of various Sn, C, O, and H containing chemical compounds was estimated at temperatures between 0 °C and 1,200 °C. The initial equilibrium simulations were performed with 1 kmol of SnO_2 balanced with increasing amount of H_2 or alkanes. The T_{100} of several commercially accessible alkanes ($C_xH_{y=2x+2}$, $0 \le x \le 4$), methane (CH_4), ethane (C_2H_6), propane (C_3H_8), and butane (C_4H_{10}), were measured and compared with that of pure H_2 to estimate the effect of carbon addition on the reducing power of a gas phase reductant. To generalize the effect of carbon, the measured T_{100} values were fitted to exponential curves.

Density functional theory calculation. We performed density functional theory calculations with the Vienna ab-initio simulation package (VASP)[27] with the Perdew-Burke-Ernzerhof (PBE)[28] exchange-correlation functional to study the reaction pathway and the corresponding energetics of alkane ($C_xH_{y=2x+2}$, $0 \le x \le 4$) reduction of SnO_2. The most bottom SnO_2 triple layer was fixed during the optimization to ensure the structural robustness of the slab models. The interaction between the ionic cores and the valence electrons was described with the projector augmented-wave method[29]. The valance-electron wave functions were expanded in the plane-wave basis set up to the energy cutoff of 400 eV. The convergence criteria for the electronic structure and the atomic geometry were 10^{-4} eV and 0.03 eV/Å, respectively.

The datasets generated during and/or analyzed during the current study are available from the corresponding author on reasonable request.

Received: 2 January 2019; Accepted: 31 October 2019;
Published online: 13 November 2019

References

1. Gupta, B., Mudhar, N. & Singh, I. Separations and recovery of indium and gallium using bis(2,4,4-trimethylpentyl)phosphinic acid (Cyanex 272). *Sep. Purif. Technol.* **57**, 294–303 (2007).
2. Mitchell, A. R. & Parker, R. H. The reduction of SnO_2 and Fe_2O_3 by solid carbon. *Miner. Eng.* **1**, 53–66 (1988).
3. Rimaszeki, G., Kulcsar, T. & Kekesi, T. Application of HCl solutions for recovering the high purity metal from tin scrap by electrorefining. *Hydrometallurgy* **125**, 55–63 (2012).
4. Rabah, M. A. Combined hydro-pyrometallurgical method for the recovery of high lead/tin/bronze alloy from industrial scrap. *Hydrometallurgy* **47**, 281–295 (1998).
5. Li, Y., Liu, Z., Li, Q., Liu, Z. & Zeng, L. Recovery of indium from used indium–tin oxide (ITO) targets. *Hydrometallurgy* **105**, 207–212 (2011).
6. Kim, S.-K., Lee, J.-C. & Yoo, K. Leaching of tin from waste Pb-free solder in hydrochloric acid solution with stannic chloride. *Hydrometallurgy* **165**, 143–147 (2016).
7. Kang, H. N., Lee, J.-Y. & Kim, J.-Y. Recovery of indium from etching waste by solvent extraction and electrolytic refining. *Hydrometallurgy* **110**, 120–127 (2011).
8. Jun, W. S., Yun, P. S. & Lee, E. C. Leaching behavior of tin from Sn–Fe alloys in sodium hydroxide solutions. *Hydrometallurgy* **73**, 71–80 (2004).
9. Itoh, S. & Maruyama, K. *In High Temp. Mater. Processes* **30**, 317–322 (2011).
10. Dattoli, E. N., Davydov, A. V. & Benkstein, K. D. Tin oxide nanowire sensor with integrated temperature and gate control for multi-gas recognition. *Nanoscale* **4**, 1760–1769 (2012).
11. Nayral, C. *et al*. A Novel Mechanism for the Synthesis of Tin/Tin Oxide Nanoparticles of Low Size Dispersion and of Nanostructured SnO_2 for the Sensitive Layers of Gas Sensors. *Adv. Mater.* **11**, 61–63 (1999).
12. Cho, M. G., Kim, H. Y., Seo, S.-K. & Lee, H. M. Enhancement of heterogeneous nucleation of β-Sn phases in Sn-rich solders by adding minor alloying elements with hexagonal closed packed structures. *Appl. Phys. Lett.* **95**, 021905 (2009).
13. Nah, J.-W., Kim, J. H., Lee, H. M. & Paik, K.-W. Electromigration in flip chip solder bump of 97Pb–3Sn/37Pb–63Sn combination structure. *Acta Mater.* **52**, 129–136 (2004).
14. Betz, U., Kharrazi Olsson, M., Marthy, J., Escolá, M. F. & Atamny, F. Thin films engineering of indium tin oxide: Large area flat panel displays application. *Surf. Coat. Technol.* **200**, 5751–5759 (2006).
15. Ginley, D. S. & Bright, C. Transparent conducting oxides. *MRS Bull.* **25**, 15–18 (2000).
16. Bae, J.-Y., Park, J., Kim, H. Y., Kim, H.-S. & Park, J.-S. Facile Route to the Controlled Synthesis of Tetragonal and Orthorhombic SnO_2 Films by Mist Chemical Vapor Deposition. *ACS Appl. Mater. Inter.* **7**, 12074–12079 (2015).
17. https://www.lme.com.
18. https://www.itri.co.uk/sustainability/material-flow-and-recycling.
19. Wright, P. A. *Extractive metallurgy of tin*. (Elsevier Scientific Pub. Co., 1982).
20. Han, T. *et al*. Modification of the Amount of CH_4 Supplied for the Efficient CH_4 Reduction of SnO_2. *Korean J. Met. Mater.* **56**, 384–391 (2018).
21. Ha, H. *et al*. Design of Reduction Process of SnO_2 by CH_4 for Efficient Sn Recovery. *Sci. Rep.* **7**, 14427 (2017).
22. Upham, D. C. *et al*. Catalytic Molten Metals for the Direct Conversion of Methane to Hydrogen and Separable Carbon. *Science* **358**, 917–921 (2017).
23. Active thermochemical tables, version 1.122g, https://atct.anl.gov.
24. Ha, H., Yoon, S., An, K. J. & Kim, H. Y. Catalytic CO Oxidation over Au Nanoparticles Supported on CeO_2 Nanocrystals: Effect of the Au-CeO_2 Interface. *ACS Catal.* **8**, 11491–11501 (2018).
25. Ha, H., An, H., Yoo, M., Lee, J. & Kim, H. Y. Catalytic CO Oxidation by CO-Saturated Au Nanoparticles Supported on CeO_2: Effect of CO Coverage. *J. Phys. Chem. C* **121**, 26895–26902 (2017).
26. NIST Chemistry WebBook, NIST Standard Reference Database Number 69, https://webbook.nist.gov/chemistry.
27. Kresse, G. & Furthmuller, J. Efficiency of ab-initio Total Energy Calculations for Metals and Semiconductors Using a Plane-Wave Basis Set. *Comput. Mater. Sci.* **6**, 15–50 (1996).
28. Perdew, J. P., Burke, K. & Ernzerhof, M. Generalized Gradient Approximation Made Simple. *Phy. Rev. Lett.* **77**, 3865–3868 (1996).
29. Blochl, P. E. Projector Augmented-Wave Method. *Phys. Rev. B* **50**, 17953–17979 (1994).

Acknowledgements

This work was supported by the National Research Foundation of Korea (NRF) funded by the Ministry of Science and ICT (2017R1A2B4009829 and 2017R1A4A1015360). This work was conducted under the framework of the research and development program of the Korea Institute of Energy Research (B92441). H.H. thanks to the support by the NRF (National Research Foundation of Korea) Grant funded by the Korean Government (NRF-2018-Fostering Core Leaders of the Future Basic Science Program/Global Ph.D. Fellowship Program). This research used resources of the Center for Functional Nanomaterials, which is a U.S. DOE Office of Science Facility, and the Scientific Data and Computing Center, a component of the Computational Science Initiative, at Brookhaven National Laboratory under Contract No. DE-SC0012704. Computing time was also provided by the National Institute of Supercomputing and Network/Korea Institute of Science and Technology Information (KSC-2018-CRE-0078).

Author contributions

H.Y.K. designed this work. M.Y., H.A. and H.H. performed thermodynamic simulations and density functional theory calculations. H.C. and E.K. analyzed the results. H.Y.K. wrote the manuscript. All the authors contributed to discuss on the manuscript.

Competing interests

The authors declare no competing interests.

Additional information

Correspondence and requests for materials should be addressed to H.Y.K.

Reprints and permissions information is available at www.nature.com/reprints.